High temperature cavity polaritons in epitaxial Er_2O_3 on silicon

C. P. Michael,[1,a)] V. A. Sabnis,[2] H. B. Yuen,[2] A. Jamora,[2] S. Semans,[2] P. B. Atanackovic,[2] and O. Painter[1]
[1]*Department of Applied Physics, California Institute of Technology, Pasadena, California 91125, USA*
[2]*Translucent, Inc., 952 Commercial St., Palo Alto, California 94303, USA*

(Received 17 November 2008; accepted 7 March 2009; published online 1 April 2009)

Cavity polaritons around two Er^{3+} optical transitions are observed in microdisk resonators fabricated from epitaxial Er_2O_3 on Si(111). Using a pump-probe method, spectral anticrossings and linewidth averaging of the polariton modes are measured in the cavity transmission and luminescence at temperatures above 361 K. © *2009 American Institute of Physics*. [DOI: 10.1063/1.3109791]

On-chip optical interconnects with wavelength division multiplexing are being pursued as a low-power low-latency high-bandwidth alternative to metal interconnects.[1] Significant research has focused on integrating optical gain material into the Si platform, with III-V wafer bonding to Si being the most successful candidate to date.[2] In addition there is a long history of efforts to incorporate Er^{3+} into Si material systems for light emission and optical gain. Erbium-doped fibers are the dominant amplifiers for telecommunications because of their high quantum efficiency and because the shielded Er^{3+} $4f$ transition wavelengths are largely insensitive to temperature and the host matrix.[3] However, the small gain coefficient of Er^{3+}-doped materials is insufficient for dense microphotonic applications.[4] To compensate for erbium's small emission cross section, stoichiometric erbium compounds are potential alternatives that achieve Er^{3+} densities 100 times greater than erbium's solubility limit in doped materials.[5–8] The high density and weak inhomogeneous broadening of stoichiometric erbium crystals can intrinsically produce large dispersive resonances in the refractive index and vacuum-Rabi splitting of optical cavity modes.[9]

Rabi splitting and the associated cavity-polariton modes can be described as a consequence of linear dispersion or as nonperturbative coupling between the dipole(s) and an optical cavity, while perturbative coupling to a single ion produces Purcell-enhanced emission.[10] For rare-earth emitters, cavity polaritons have been observed around a single Er^{3+} transition in an oxidized polycrystalline erbium layer,[11] but the effect was quenched at $T \gtrsim 40$ K.[12] We have previously shown that atomic layer epitaxy produces high quality single-crystal Er_2O_3 films on silicon and offers the prospect of electrical injection through precisely controlled heterostructures.[8] In this letter, we describe the spectroscopy of small mode-volume Er_2O_3 microdisk resonators formed from this material, and we analyze the properties of high temperature ($T > 361$ K) cavity polaritons formed between the cavity's whispering-gallery modes (WGMs) and two Er^{3+} transitions in the 1500 nm band.

Analyzing the polariton response involves continuously tuning a cavity mode across the Er^{3+} transitions. As a mode is shifted through an optical transition, the resonances anticross (i.e., the vacuum-Rabi splitting) and produce symmetric hybrid modes (i.e., the cavity polaritons), which appear in both the cavity transmission and photoluminescence (PL). In terms of cavity quantum electrodynamics (cQED), the fundamental quantity for cavity polaritons is the Rabi frequency that describes the coherent coupling between the two-level system(s) and a near-resonant optical mode. For a uniform distribution of emitters, the many-dipole Rabi frequency ($\bar{g}_N$) is given by

$$|\bar{g}_N|^2 = N|\bar{g}_1|^2 \approx \frac{|\vec{\mu}|^2 \omega_c \rho \Gamma}{2\hbar n^2 \epsilon_0}, \tag{1}$$

where $\bar{g}_1$ is the mean coupling rate experienced by a single dipole, N is the number of dipoles in the cavity, $\vec{\mu}$ is the electric dipole moment of the optical transition, $\omega_c(\lambda_c)$ is the frequency (wavelength) of the cavity resonance, n is the refractive index of the dipole medium, $\rho \approx N/(V_m \Gamma)$ is the dipole density in Er_2O_3, $V_m \approx 70(\lambda_c/n)^3$ is the optical mode volume, and Γ is the optical mode's electric-field energy overlap with the dipole ensemble.[13,14] In Er_2O_3 resonators, a large Er^{3+} density overcomes the small ${}^4I_{13/2} \rightarrow {}^4I_{15/2}$ dipole moment to produce resolved cavity polaritons.

Microdisk cavities are fabricated from a 150 nm thick Er_2O_3 film grown on Si(111) using the methods in Ref. 8. The resulting resonators suffer little surface scattering (Fig. 1) and have quality factors (Q) on the order of 10^3 due to the

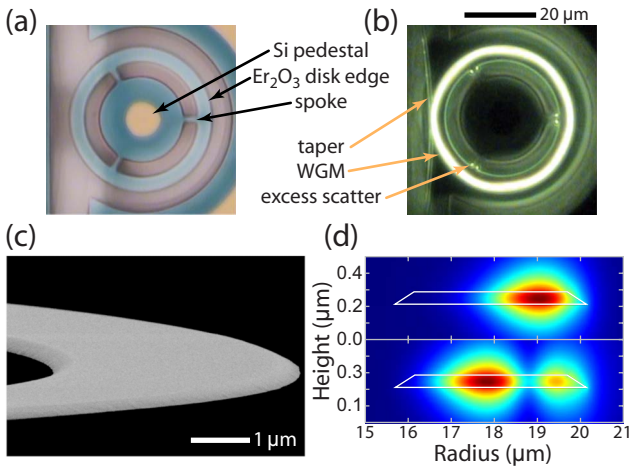

FIG. 1. (Color online) (a) Optical image of a spoked Er_2O_3 microdisk. (b) Visible upconversion luminescence shows the spatial profile of a fundamental mode and additional scattering where the spokes attach to the ring. (c) Scanning electron micrograph showing the smooth edge of an undercut microdisk. (d) Electric-field profile ($|E|^2$) of the first- and second-order radial modes calculated using the finite element method.

a)Electronic addresses: cmichael@caltech.edu.

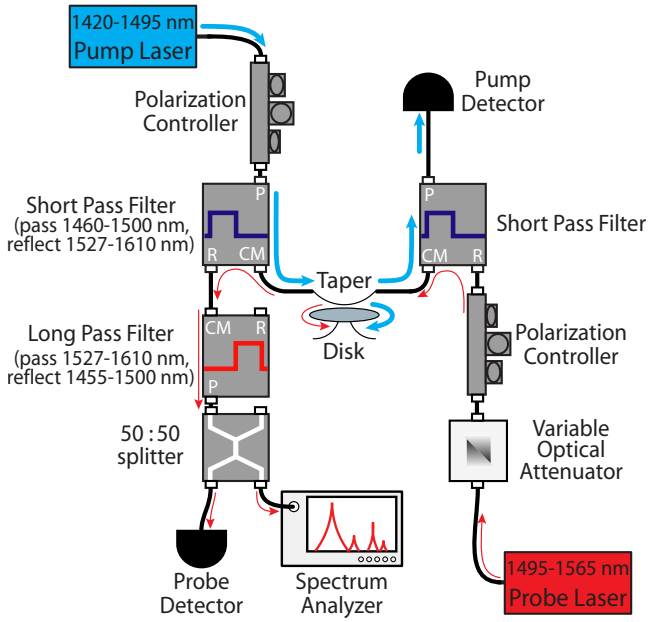

FIG. 2. (Color online) Schematic layout for pump-probe measurements.

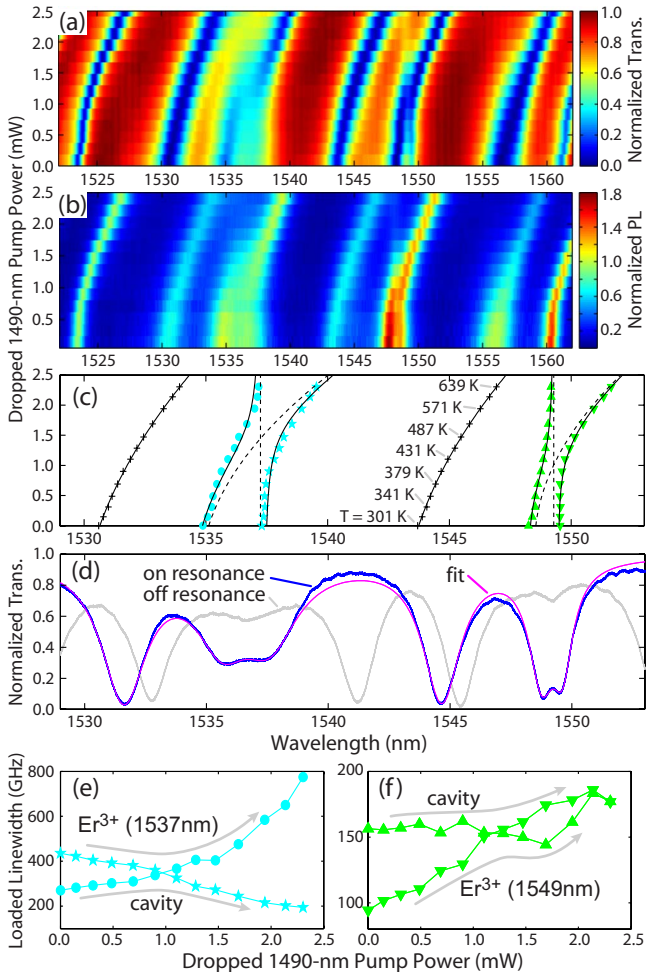

FIG. 3. (Color online) (a) Normalized probe transmission and (b) PL as a function of wavelength and pump power. To compensate for upconversion effects, the PL spectra are normalized to give a constant value for the peak near 1525 nm. (c) Comparison of measured resonance wavelengths, the coupled-oscillator eigenvalues (solid lines), and the uncoupled transition and cavity responses (dashed lines). The device temperature is inferred from the bare cavity mode detuning and a constant tuning rate of 9.7 pm/K. (d) Transmission for two devices tuned on and off resonance with the Er^{3+} transitions; a sample fit is also included. [(e) and (f)] Linewidth averaging of the polariton modes.

resonant Er^{3+} absorption. We use a fiber-taper waveguide and tunable diode lasers to analyze the WGM spectrum and efficiently pump/collect the Er^{3+} PL. The temperature dependence of the refractive index offers a convenient and reversible means to tune the microdisk resonances, but the low tuning rate for these modes (9.7 pm/K, corresponding to $dn/dT=1.9\times10^{-5}$ K^{-1}) limits the wavelength range for simply heating the entire sample (maximum $\Delta\lambda\approx0.6$ nm for $\Delta T\approx60$ K). Instead, we use optical absorption and the low thermal conductivity associated with undercut microcavities to locally heat the optical mode volume of a single device. To obtain a wide tuning range, we further decrease the resonator's thermal conductivity by fabricating microdisks with three thin spokes supporting a 4 μm wide ring where the mode resides [Fig. 1(a)]. The spokes, nominally 2 μm wide, incur some additional scattering [Fig. 1(b)] but only marginally degrade the Q of the fundamental WGMs—the second-order WGMs experience higher scattering losses due to greater overlap with the spokes [Fig. 1(d)]. With 3.6 mW of pump power, we are able to redshift a WGM from 1489.8 to 1495.5 nm. Assuming that the thermo-optic coefficient of Er_2O_3 rate remains constant, the 5.7 nm change corresponds to $\Delta T=590$ K and a final temperature of $T=890$ K; currently we have no method to verify temperatures above ~375 K.

To tune the resonator and observe the anticrossing, we perform a counterpropagating pump/probe measurement that simultaneously heats the cavity, monitors the cavity transmission, and collects the Er^{3+} luminescence (Fig. 2). The counterpropagating configuration and edge-pass filters combine/split the beams with <1 dB loss and provide >100 dB pump-probe isolation at the probe detector and optical spectrum analyzer. Unlike many cQED experiments that must minimize V_m, the uniform dipole density for planar microdisks [see Eq. (1)] makes $\bar{g}_N$ independent of V_m so Γ and ρ become more important design parameters. For these experiments, a microdisk radius of ~20 μm is chosen so that the quasi-TE mode spectrum consists of evenly spaced first- and second-order radial modes—$\Gamma=0.67$ and has a weak dependence on radius. The cavities' radii are also varied slightly to acquire a device with first-order WGMs slightly blue detuned from the polariton features at 1537 and 1549 nm. With the fiber-taper input/collection waveguide in contact with the disk to stabilize the coupling against mechanical noise, we pump a fundamental WGM near 1490 nm with 0.5–2.5 mW in the clockwise direction to heat the disk and drive the $^4I_{13/2}\leftrightarrow{}^4I_{15/2}$ transition. While the 1490 nm pump laser is tuned to maximize the dropped pump power, a second ~200 nW tunable laser probes the cavity's transmission spectrum in the counterclockwise direction. The C-band PL is also measured by simply blocking this probe beam.

As the cavity is heated, the split resonances clearly anticross in both transmission [Fig. 3(a)] and PL [Fig. 3(b)] while the bare cavity modes tune as a quadratic polynomial of the pump power—the nonlinearity stems from Er^{3+} cooperative upconversion which produces a cascade of multiphonon transitions. Parts of these anticrossings are also observed in separate measurements when we heat the sample stage from 300 to 361 K, but, as discussed previously, this

temperature range is insufficient to tune a cavity mode completely across the Er^{3+} transitions. In both measurements when the cavity modes are detuned from the Er^{3+} transitions as in Fig. 3(d), weak transmission features remain near the polariton resonance wavelengths that have no cavitylike character and are due to single-pass loss in the taper waveguide as it evanescently senses the sharp Er_2O_3 absorption spectrum.

In addition to the spectral anticrossing, the linewidths of the polariton branches average as the cavity modes and Er^{3+} lines become resonant, further indicating the hybridization of the photonic and atomic degrees of freedom. For each trace in Fig. 3(a), we fit a series of Lorentzian valleys [Fig. 3(d)] to extract the resonances' loaded linewidths and demonstrate that they become equal near the anticrossing for both sets of polaritons [Figs. 3(e) and 3(f)]. At higher pump powers (higher cavity temperature), the widths of the Er^{3+} lines broaden, which is likely due to added phonon-related dephasing.[15]

To quantitatively describe the polaritons and obtain $\bar{g}_N$, we diagonalize and fit a coupled-oscillator Hamiltonian to the eigenfrequencies in Fig. 3(a). Assuming that the quasi-TE cavity modes are linearly polarized, $\bar{g}_N$ becomes real, and we use five parameters for the tuning of each cavity-polariton pair: $\bar{g}_N$, the Er^{3+} transition wavelength (λ_0), and the three coefficients that describe the quadratic tuning of the bare cavity mode. The fit in Fig. 3(c) gives $\bar{g}_N/2\pi$ of 99 and 57 GHz for the Er^{3+} transitions at 1537.2 and 1549.2 nm, respectively. As evident in comparing peaks across Fig. 3(b), the coupling to each ion is weak ($\bar{g}_1/2\pi \approx 0.3$ MHz and 0.1 MHz for $N \approx 10^{11}$) and does not increase the material's emission efficiency; the 8 ms bulk radiative lifetime is much shorter than the expected Purcell lifetime $\kappa/2\bar{g}_1^2 > 150$ ms, where κ is the cavity field decay rate.[10] The $\bar{g}_1$ values also reflect the necessity of high ion densities to achieve resolved vacuum-Rabi splitting while compensating for erbium's small dipole moment. Based on the spectroscopy of Er^{3+} in Y_2O_3 (Refs. 16 and 17) and our own preliminary data at 8 K, we associate the 1537.2 and 1549.2 nm splittings with ${}^4I_{13/2} \leftrightarrow {}^4I_{15/2}$ transitions between their lowest Stark levels ($Y_1 \leftrightarrow Z_1$) on the low-symmetry C_2 and high-symmetry C_{3i} lattice sites, respectively. However, neighboring resonances between higher sublevels have significant dipole moments and may also contribute to the polariton behavior—e.g., the $Y_2 \leftrightarrow Z_2$ (C_2) and $Y_3 \leftrightarrow Z_3$ (C_{3i}) transitions near 1537 and 1549 nm, respectively.[16] Using the absorption data in Ref. 8 to estimate the effective transition matrix elements under weak excitation and the density of the C_2 and C_{3i} sites (2.04×10^{22} and 6.80×10^{21} cm^{-3}, respectively), Eq. (1) gives $\bar{g}_N/(2\pi) = 109$ and 33 GHz at 1537 and 1549 nm, respectively. Since energy migration to quenching sites is the dominant mechanism for nonradiative decay, the discrepancy between the measured and estimated $\bar{g}_N$ values and the higher PL efficiency at 1549 nm may reflect a useful asymmetry in the diffusion through the C_{3i} and C_2 sites. We are also working to understand why high temperature polaritons only form around $Y_1 \leftrightarrow Z_1$ transitions and not around transitions involving higher Stark levels with similar absorption peaks.

The robust collective coupling we have observed between two Er^{3+} transitions and the optical modes in Er_2O_3 resonators is an appealing route to improving the material's efficiency or gain through cQED effects, such as cavity-enhanced super-radiance[18] and the Purcell Effect. Unfortunately to achieve super-radiant emission, with yield increasing as N^2, the ensemble must be excited into a Dicke state that quickly decoheres due to fast dephasing above cryogenic temperatures.[19] Because collective relaxation of the polariton modes is difficult to initiate, Purcell-enhanced emission from individual Er^{3+} ions is a more promising direction and can be realized by decreasing V_m.[10,13] By integrating proposed ultrasmall mode volumes formed using nanoscale slots[20] with recent low-loss photonic crystals in Si,[21] a hybrid Si cavity containing an Er_2O_3 slot ($\Delta n \approx 1.5$, $V_m \approx 0.18(\lambda/n)^3$, $Q \approx 10^6$, and $\kappa/2\pi \approx 100$ MHz) could exhibit an enhanced emission lifetime of 0.23 μs, compared to a 7.2 μs nonradiative lifetime. Further investigations of these cavity polaritons are in progress to explore enhanced emission, the different dynamics of Er^{3+} ions on C_2 and C_{3i} sites, and methods to suppress nonradiative quenching within these crystals.

[1] M. J. Kobrinsky, B. A. Block, J.-F. Zheng, B. C. Barnett, E. Mohammed, M. Reshotko, F. Roberton, S. List, I. Young, and K. Cadien, Intel Technol. J. **8**, 129 (2004).
[2] A. W. Fang, H. Park, O. Cohen, R. Jones, M. J. Paniccia, and J. E. Bowers, Opt. Express **14**, 9203 (2006).
[3] E. Desurvire, *Erbium-doped Fiber Amplifiers: Principles and Applications* (Wiley, New York, 2002).
[4] *Silicon Photonics*, Topics in Applied Physics Vol. 94, edited by L. Pavesi and D. J. Lockwood (Springer, Berlin, 2004).
[5] H. Isshiki, M. J. A. de Dood, A. Polman, and T. Kimura, Appl. Phys. Lett. **85**, 4343 (2004).
[6] A. M. Grishin, E. V. Vanin, O. V. Tarasenko, S. I. Khartsev, and P. Johansson, Appl. Phys. Lett. **89**, 021114 (2006).
[7] K. Suh, J. H. Shin, S.-J. Seo, and B.-S. Bae, Appl. Phys. Lett. **89**, 223102 (2006).
[8] C. P. Michael, H. B. Yuen, V. A. Sabnis, T. J. Johnson, R. Sewell, R. Smith, A. Jamora, A. Clark, S. Semans, P. B. Atanackovic, and O. Painter, Opt. Express **16**, 19649 (2008).
[9] Y. Zhu, D. J. Gauthier, S. E. Morin, Q. Wu, H. J. Carmichael, and T. W. Mossberg, Phys. Rev. Lett. **64**, 2499 (1990).
[10] H. J. Carmichael, *Statistical Methods in Quantum Optics 2* (Springer, Berlin, 2008).
[11] M. Lipson and L. C. Kimerling, Appl. Phys. Lett. **77**, 1150 (2000).
[12] M. Lipson and L. C. Kimerling, Opt. Mater. (Amsterdam, Neth.) **16**, 47 (2001).
[13] H. J. Kimble, Phys. Scr., T **T76**, 127 (1998).
[14] Y. Colombe, T. Steinmetz, G. Dubois, F. Linke, D. Hunger, and J. Reichel, Nature (London) **450**, 272 (2007).
[15] E. Desurvire, J. L. Zyskind, and J. R. Simpson, IEEE Photonics Technol. Lett. **2**, 246 (1990).
[16] J. B. Gruber, K. L. Nash, D. K. Sardar, U. V. Valiev, N. Ter-Gabrielyan, and L. D. Merkle, J. Appl. Phys. **104**, 023101 (2008).
[17] The difference between the observed and reported wavelengths (1535.4 and 1547.7 nm in Ref. 16) is due to drift in our laser's wavelength calibration.
[18] M. Gross, P. Goy, C. Fabre, S. Haroche, and J. M. Raimond, Phys. Rev. Lett. **43**, 343 (1979).
[19] C. Greiner, B. Boggs, and T. W. Mossberg, Phys. Rev. Lett. **85**, 3793 (2000).
[20] J. T. Robinson, C. Manolatou, L. Chen, and M. Lipson, Phys. Rev. Lett. **95**, 143901 (2005).
[21] Y. Takahashi, H. Hagino, Y. Tanaka, B.-S. Song, T. Asano, and S. Noda, Opt. Express **15**, 17206 (2007).